Analysis of Crack Propagation in Asphalt Concrete Using Cohesive Crack Model

YEOU-SHANG JENQ AND JIA-DER PERNG

A cohesive crack model, which is similar to the Dugdale-Barenblatt model, was proposed to simulate the progressive crack development in asphalt concrete. Tensile strength, fracture energy, and the stress-separation relationship are the basic material properties associated with this model. To evaluate the material properties, indirect tensile tests and three-point bend tests were performed. From these experimental results, the effects of temperature on Young's modulus, the fracture energy, and the indirect tensile strength were evaluated. To determine the stress-separation relationship, a numerical simulation (or curve-fitting method) was used. Using the material properties obtained from the experimental study, temperature effects on different fracture parameters (i.e., critical stress intensity factor and critical J-integral) were studied. The theoretical predictions were found to be in good agreement with the available experimental results. This finding also indicates the potential applications of the proposed model in evaluating the performance of asphalt concrete pavements.

Asphalt concrete is composed of brittle inclusions (aggregates) and viscous matrix (asphalt cement). Because of the viscous matrix, asphalt concrete behaves like a viscoelastic material. As a result, the stress-strain response depends on the loading rate and the environmental temperature. A basic understanding of the time-dependent response of asphalt concrete can be qualitatively obtained by the use of rheological models. The simplest model is the Maxwell model, which consists of a spring (providing the elastic response) and a dashpot (providing the viscous response) connected in series. A more realistic representation of actual behavior of asphalt concrete can be modeled using the Burger model (*1*). In general, the strain (ε) of a viscoelastic material such as asphalt concrete can be expressed as a function of time (t), temperature (T), and loading rate $\dot{\sigma}$. That is,

$$\varepsilon = \varepsilon(t,T,\dot{\sigma}) \tag{1}$$

However, it should be noted that Equation 1 is valid only for undamaged materials. To model crack propagation in asphalt concrete, a separate criterion is necessary.

FRACTURE CRITERIA

Selection of fracture criteria, which can be used to estimate the fracture strength and service life of a structure, is an important aspect of pavement design. For example, the existence of joints and cracks often causes stress concentration as well as a redistribution of stress. As a result, the failure strength predicted using a conventional strength criterion—namely, that a material will fail if the tensile strength is exceeded—may not be reliable and may overestimate the actual strength of the structure. Therefore, to properly estimate the fracture resistance of asphalt concrete, a fracture mechanics concept must be incorporated.

The distribution of the stresses in front of a crack tip (σ_{ij}) (only Mode I tensile condition is considered here) can be expressed by the following equation:

$$\sigma_{ij} = \frac{K_I}{(2\pi x)^{1/2}} + \text{higher order terms} \tag{2}$$

where

x = distance from the crack tip,
K_I = Mode I stress intensity factor, and
σ_{ij} = near tip stresses.

K_I is a function of the applied load, the crack length, and the shape of the specimen. Equation 2 indicates that the stresses around the crack tip are square-root singular. This also implies that a material with a crack cannot sustain any applied load if one assumes the strength criterion. However, it has been observed that a material with flaws or sharp cracks still has the ability to resist a certain amount of applied loads. This observation clearly indicates that a conventional strength criterion is not appropriate in estimating the crack resistance of asphalt concrete.

To overcome the drawbacks of strength criteria, Griffith (*2*) proposed a constant surface energy concept in 1921. He proposed that a brittle body fails because of the presence of many internal cracks or flaws that produce local stress concentration. He stated that the elastic body under stress must transfer from an undamaged state to a damaged state by a process during which a decrease of the potential energy takes place. He also stated that fracture instability is reached when the increase in surface energy, which is generated by the extension of the crack, is balanced by the release of elastic-strain energy in the volume surrounding the crack. For an infinitely large plate with an initial crack length of $2a$ and subjected to a uniform tension, σ_0, Griffith's energy criterion for crack propagation can be presented mathematically as

$$\delta U \geq \delta U_{SE} \tag{3}$$

where δU is the decrease in potential energy due to increased crack surface and δU_{SE} is the increase in surface energy due to increased crack surface.

Department of Civil Engineering, Ohio State University, Columbus, Ohio 43210.

The expression for the critical stress (σ_c) at which a crack will propagate based on the Griffith energy criterion can be written as

$$\sigma_0 = \sigma_c \text{ (crack driving force = fracture resistance)} \quad (4)$$

and

$$\sigma_c = \left(\frac{2\tau E}{\pi a}\right)^{1/2} \quad (5)$$

where τ is surface energy per unit area, and E is Young's modulus.

According to Irwin (*3*), the following relation can be derived between the Mode I stress intensity factor (K_I) and the energy release rate (G):

$$K_I = (EG)^{1/2} \text{ for plane stress case} \quad (6)$$

$$K_I = \left(\frac{EG}{1-\nu^2}\right)^{1/2} \text{ for plane strain case} \quad (7)$$

Because the energy release rate is two times that of the Griffith surface energy, the critical stress intensity factor (K_{Ic}) and critical energy release rate (G_c) can be used as crack propagation criteria.

The Griffith energy criterion is based on linear-elastic fracture mechanics (LEFM) assumptions, that is, there is no (or negligible) plastic deformation in the material. However, for most materials, inelastic deformation such as plastic deformation always takes place. Thus, the Griffith criterion must be modified for materials with significant inelastic deformation. Orowan (*4*) and Irwin and Kies (*5*) concluded that even a slight plastic flow that occurs in the brittle fracture case will absorb a great amount of additional energy required to create new surfaces.

Irwin and Kies also recognized that the plastic energy dissipated in material is much higher than the surface energy dissipated. Therefore, they proposed that the surface energy can be neglected when compared with plastic energy. To simulate this type of nonlinear energy dissipation, a cohesive crack model was proposed by Dugdale (*6*) and Barenblatt (*7*).

Dugdale Model

To simulate the plastic fracture process observed in a thin metal plate, Dugdale (*6*) proposed a model that assumed that the length of the plastic zone is much larger than the thickness of the sheet and that the plastic zone is a yielded strip ahead of the crack tip. The material is assumed to be elastic—perfectly plastic so that the stress within the yielded strip equals the yield strength (σ_y). Dugdale also postulated that the effect of yielding is to increase the crack length by the extent of the plastic zone, as shown in Figure 1 for a finite length crack in an infinite medium subjected to a uniform remote stress (σ_0). Within the yielded strip (a_c), the opening of the crack faces is restrained by the closing pressure (or yield stress) (σ_y). The length (d) of this strip can be determined from the condition that the stress field is nonsingular.

By superposing the solutions for the uncracked sheet loaded by a remote tension (σ_0), and for the cracked sheet with

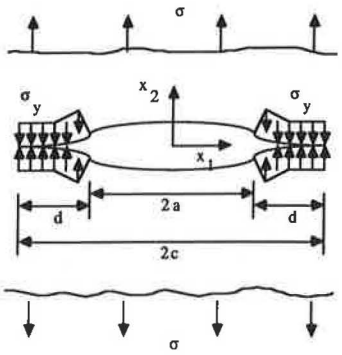

FIGURE 1 Dugdale model.

remote loading and with pressure $p_2(x) = \sigma_0$ for $|x| \le a$ and $p_2 = \sigma_0 - \sigma_y$ for $a \le |x| \le c$ on the crack surface (Figure 1), Dugdale came to an expression for the length of the plastic zone:

$$d = 2a \cdot \sin^2\left(\frac{\pi\sigma_0}{4\sigma_y}\right) = \frac{\pi}{8}\left(\frac{K_I}{\sigma_y}\right)^2 \quad (8)$$

He found very good agreement between the measured lengths of the plastic zones in steels from experimental results and the predictions based on Equation 8 for σ_0 as large as $0.9\sigma_y$. It should be noted that the specific energy dissipation for crack formation in this model is unbounded, which is not a reasonable assumption for most materials.

Barenblatt Model

As in the Dugdale model, Barenblatt (*7*) proposed that a cohesive force acts across a fracture process zone ahead of the real crack tip. However, unlike the yielding consideration assumed by Dugdale, the cohesive force in the Barenblatt model is from molecular force consideration, and the cohesive force depends on the opening displacement along the crack. As a result, specific energy dissipation for crack formation is bounded, which is a more realistic assumption.

The cohesive crack concept was later successfully extended by Hillerborg et al. (*8*) to study nonlinear fracture process in portland cement concrete.

COHESIVE CRACK MODEL FOR ASPHALT CONCRETE

To properly model the crack propagation in asphalt concrete, a cohesive crack model, which is similar to the Dugdale-Barenblatt model, is proposed. Some fundamental concepts and basic assumptions regarding the proposed cohesive crack model are discussed first.

Basic Assumptions

To simulate the fracture process using the Dugdale-Barenblatt cohesive crack model, the following assumptions were made:

1. The process zone starts to develop at one point when the first principal stress reaches the tensile strength f_t.
2. The process zone develops perpendicular to the direction of first principal stress.
3. The properties of the materials outside the process zone are governed by stress-strain (σ-ε) relation (e.g., Equation 1 or Figure 2).
4. The material in the process zone is able to transfer stress, and the stress-transferring capability depends on its opening according to the stress-separation (σ-w) curve shown in Figure 3. In addition, this stress-separation relationship depends on the loading rate and the service temperature.

Based on this assumption, the specific energy dissipation can be shown to be bounded, which is a reasonable assumption. An example of the closing pressure along this process zone can be modeled as nonlinear spring coupled with dashpots (see Figure 4).

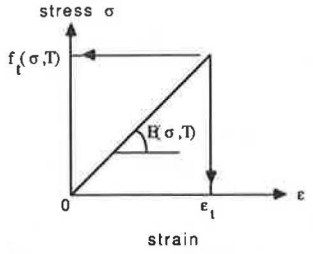

FIGURE 2 Straight line approximation of the σ-ε curve for asphalt concrete.

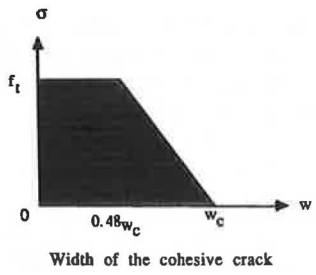

FIGURE 3 Bilinear simulation of σ-w curve for asphalt concrete.

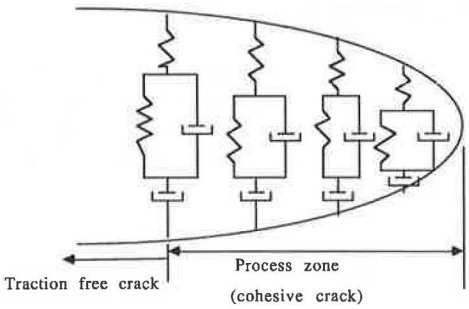

FIGURE 4 Cohesive crack modeled by Burger model.

To obtain the theoretical results using the proposed cohesive crack model, a numerical method such as finite element methods must be applied.

Numerical Formulation

For simplicity, a notched beam is used to demonstrate the numerical formulation. Consider a notched beam with a preexisting crack up to node n subjected to a load P in the midspan, as shown in Figure 5. It is assumed that the process zone will develop along a straight plane, which is reasonable for Mode I crack propagation. When the beam is loaded, by introducing the closing stresses over the crack, one can analyze the progressive crack development in the beam.

In the calculation process, the stresses acting across the cohesive crack were replaced by equivalent nodal forces. These forces can be determined according to the stress-separation (σ-w) curve when the width at the cohesive crack zone is known. As shown in Figure 5, when the first node reaches its tensile strength, the opening at the first node is still equal to zero, that is, $\sigma_1 = f_t$, $w_1 = w_2 = \ldots = w_{n-1} = 0$. From this, one can determine the first point, which corresponds to the crack initiation point of the load-load line deflection (P-δ) curve and the load-crack mouth opening displacement (P-CMOD) curve.

When the crack starts to propagate, as shown in Figure 6, the first node is opened and the second node is assumed to

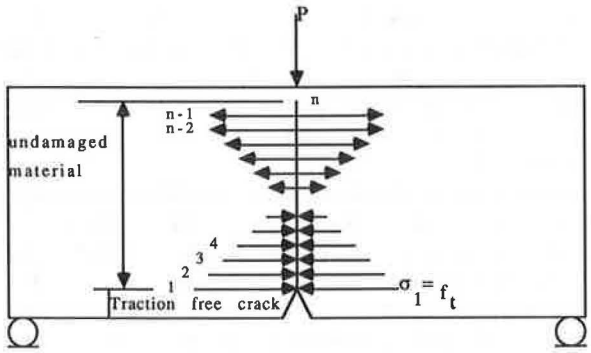

FIGURE 5 Schematic illustration of first step of numerical calculation.

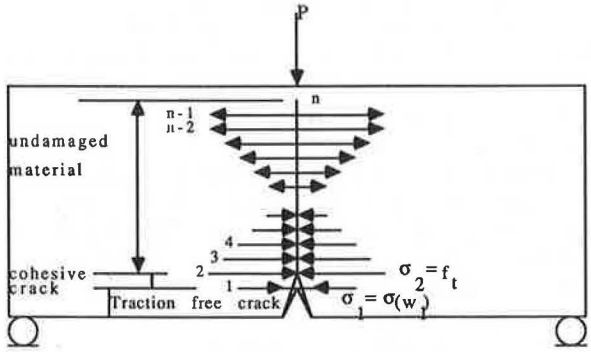

FIGURE 6 Schematic illustration of second step of numerical calculation.

reach the tensile strength. At this point the boundary conditions can be expressed as $\sigma_2 = f_t$, $w_2 = w_3 = \ldots w_{n-1} = 0$, $w_1 \neq 0$, $\sigma_1 = \sigma(w_1)$. The system equations are nonlinear because of the stress-separation constraint, that is, σ_1 depends on the value of w_1, and w_1, on the other hand, is affected by the magnitude of σ_1. Therefore, an iteration process is needed for this step.

Following the same procedure, the progress of the crack propagation can be analyzed and the complete P-δ curve and P-CMOD curve can be generated. More detailed numerical formulation is given elsewhere (*9*).

MATERIAL PROPERTIES

An experimental program is designed to evaluate the material properties associated with the proposed model. The tensile strength, the fracture energy, and Young's modulus were determined using Marshall tablets and beam specimens.

Asphalt Concrete Mix

The asphalt cement used in this study is AC-20 grade, which was purchased from the Koch Company in Ohio. The aggregates are natural gravel and natural sand obtained locally. The gradation of the aggregate satisfies the requirement of 404 mix specified by Ohio Department of Transportation (*10*). The mixing temperature is 300°F, and the compaction temperature is 280°F. A medium traffic condition was assumed; thus, for the asphalt tablets the number of compaction blows at each end of the specimen is 50. The optimum asphalt content according to Marshall mix design is 5.15 percent. This optimum asphalt content was used to produce the asphalt tablets and the beam specimens. The asphalt tablets were used for Marshall stability tests and indirect tensile tests. The beams were used for the three-point bend tests. Some of the beams were sawcut with notch-depth ratios of 0.2, 0.4, and 0.6. The beam specimens are 15 in. long, 2.9 in. high, and 3 in. wide. The asphalt tablets are 4 in. in diameter and 3 in. high.

The tablets were prepared according to the Mix Design Method for Asphalt Concrete (MS-2) recommended by the Asphalt Institute for Marshall stability tests (*11*). The same mixing procedures were used to prepare the beam specimens. However, the beam specimens were compacted statically using a Forney testing machine by applying 10 cycles of static force to the surface of the beams. This procedure ensured that the density of the beam was similar to that of the asphalt tablets.

Indirect Tensile Tests

To measure the tensile strength of asphalt concrete, indirect tensile tests were performed (*12*). The indirect tensile tests were carried out at five temperatures: 18°F, 36°F, 75°F, 104°F, and 140°F. In the 18°F and 36°F cases, the tablets were put in the refrigerator for 1 day to reach the required temperature before testing. In the 104°F and 140°F cases, the tablets were wrapped with a plastic sheet, placed in a plastic bag, and then conditioned in the water bath for 6 hr. An MTS Systems Corporation testing apparatus was used in all of the tests. Displacement control was used to get a complete load versus load-line deflection curve. The loading rate was fixed at 0.03 in./min for the indirect tensile tests. Using this loading rate, the indirect tensile test for each asphalt tablet was finished within 10 min. Thus, the temperature change during the testing process was assumed to be negligible. The applied load and load-line deflection were monitored and recorded by an X-Y recorder. Based on the measured peak load, the indirect tensile strength can be measured and expressed as

$$f_t = \frac{2P_{\max}}{\pi DH} \tag{9}$$

where

$P_{\max}$ = measured peak load,
H = thickness of the tablet,
D = diameter of the tablet, and
f_t = indirect tensile strength.

Since the work done to fracture the specimen is equal to the area under the complete load versus load-line deflection, the fracture energy (G_F) can be expressed as

$$G_F = \left[\int_0^{\delta_{\max}} P(\delta)d\delta\right]/(HD) \tag{10}$$

The area under the P-δ curve was calculated using a planimeter.

Three-Point Bend Test

Figure 7 shows the three-point bend testing setup. The applied load and the load-line deflection were also recorded by an X-Y recorder. From the initial slope of the load-deflection curve, one can determine the modulus of elasticity. The loading rate for this test was 0.125 in./min, and the notch-depth ratios were 0.2, 0.4, and 0.6. Because the area under the load-deflection curve and the work done by the self-weight of the beam are the total energy consumed to break the beam, the fracture energy (G_F) for the beam specimens can be calculated as

$$G_F = \left[\int_0^{\delta_{\max}} p(\delta)d\delta + \frac{1}{2}Mg\delta_{\max}\right]/[(b - a)W] \tag{11}$$

where M is the mass of the beam and g is acceleration of gravity.

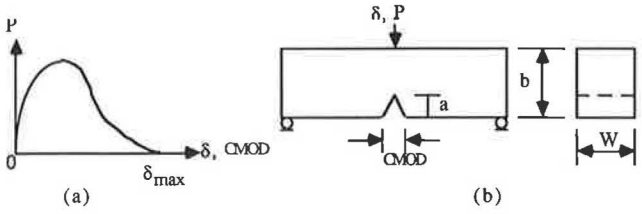

FIGURE 7 Typical P-δ and P-CMOD curves for three-point bend test.

Test Results

The results for indirect tensile tests and three-point bend tests are summarized in Tables 1 and 2. Table 1 shows that the indirect tensile strengths at different temperatures obtained from this study are comparable to the results reported by Kennedy and Hudson in 1968 (*12*). As reported by Kennedy and Hudson, the loading rate, as well as temperature, significantly affects the indirect tensile strength. A higher loading rate, as well as a lower temperature, will result in higher indirect tensile strength. Thus, the experimental results obtained from the present study (loading rate = 0.03 in./min) were judged to be reasonable (Figure 8). It can also be noted that the fracture energy increases as the temperature decreases, indicating that more energy is needed to fracture asphalt concrete at a lower temperature. This observation, at first sight, does not seem to be reasonable because asphalt concrete generally is more brittle at a lower temperature. It should be emphasized that it is the overall change of material properties that causes the brittleness of asphalt concrete observed at low temperatures. This phenomenon will be explained in the parametric study.

The fracture energy (G_F), critical stress intensity factor (K_{Ic}), and net flexural tensile strength (f_t^{net}) for different notch-depth ratios (a/b = 0.2, 0.4, and 0.6) obtained from the three-point bend tests are listed in Table 2. From this experimental study, the following material properties were extracted and are used in the present study:

1. Tensile strength (f_t): The tensile strengths obtained from the indirect tensile tests at different temperatures are used as inputs for tensile strength.
2. Fracture energy (G_F): Because of the end compressive effect of the asphalt tablets, multiple cracks were produced in the indirect tensile specimen test. As a result, the fracture energy obtained from the indirect tensile tests is higher than that obtained from the three-point bend test (Tables 1 and 2). It is therefore appropriate to select the fracture energy

TABLE 1 RESULTS OF INDIRECT TENSILE TESTS

Temp. (°F)	Specimen No.	Indirect tensile strength (f_t) (psi)	Fracture Energy (G_F) (lb/in)	Avg. f_t (psi)	Avg. G_F (lb/in)
18	0-37	293.81	18.41	305.4	19.98
	0-38	309.56	20.94		
	0-39	324.45	20.33		
	0-40	293.94	20.24		
36	0-28	183.15	17.63	189.16	18.66
	0-29	156.17	18.03		
	0-41	213.26	18.19		
	0-42	204.06	20.74		
75	0-20	70.40	9.53	63.39	8.71
	0-21	63.21	9.3		
	0-22	64.59	9.63		
	0-23	57.19	8.14		
	0-24	61.58	6.95		
104	0-33	14.07	1.65	13.70	1.54
	0-34	13.23	1.39		
	0-35	13.80	1.59		
140	0-30	3.70	0.295	3.62	0.276
	0-31	3.53	0.259		
	0-32	3.63	0.274		

TABLE 2 RESULTS OF THREE-POINT BEND TESTS (T = 75°F)

a/b ratio	Specimen No.	P_{max}[1] (lbs)	Net flexural strength	Critical stress intensity factor K_{Ic}, psi$\sqrt{in}$	Fracture Energy G_F[2] (lb/in)	Contribution[3] to G_F due to self-weight
0.2	B-0-10	177.2	203.34	173.99	2.94	0.292
	B-0-9	151.2	183.28	154.68	2.78	0.297
0.4	B-0-8	77.2	159.65	129.17	1.90	0.300
	B-0-7	64.8	128.69	105.18	2.00	0.385
0.6	B-0-6	21.2	98.64	67.51	1.33	0.456
	B-0-5	29.8	144.49	97.87	1.42	0.400
Average			153.02	121.40	2.06	0.355

1. If the self-weight of the beam is considered, an extra 5.45 lbs (i.e., one half of the weight of the beam) must be added to P_{max}.
2. Fracture energy values without the contribution of self-weight.
3. Contribution of self-weight to the fracture energy values.

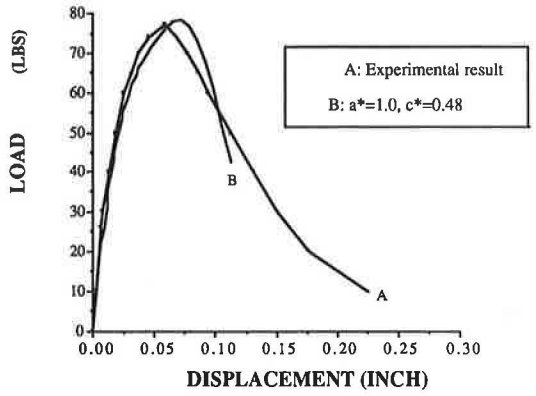

FIGURE 8 Numerical simulation of load versus load-line displacement for $a^* = 1.0$ and $c^* = 0.48$.

obtained from the three-point bend tests instead of that obtained from the indirect tensile test. However, because only the $T = 75°F$ case was performed for three-point bend tests, an alternative method is used to derive the fracture energy-temperature relationship. It was assumed that the temperature effect on G_F is the same for both indirect tensile tests and three-point bend tests. Thus, the fracture energy (G_F) of three-point bend tests can be derived as

$$G_F = 0.355 \times 10^{(1.3226 + 0.0018T - 0.0001187T^2)} \text{ lb/in.} \quad (12)$$

3. Young's modulus (E) and Poisson's ratios (ν): The Young's modulus at different temperatures can be estimated from the initial slope of the P-δ curves obtained from the indirect tensile tests as well as three-point bend tests. Young's modulus (E) was calculated using the linear-elastic fracture mechanics formulas and can be expressed as

$$E(T) = 10^{(5.93906 - 0.0142T)} \text{ psi} \quad (13)$$

Table 3 summarizes the material properties along with the characteristic length [$L_{ch} = G_F \times E/(f_t)^2$]. The effect of asphalt concrete temperature on Poisson's ratios is also included (*13*). It is worth noting that the characteristic length (L_{ch}) is a better indicator for the ductility (or brittleness) of asphaltic materials. It can be shown that the larger the characteristic length, the more ductile the material.

Determination of Stress-Separation Curve (σ-w) for Asphalt Concrete

One can determine the stress-separation relationship from a direct uniaxial tensile test. However, the experimental setup for a direct uniaxial tensile test is very sophisticated and the test results may not be reliable because of possible eccentricity involved in the experimental setup. As a result, an indirect method is used to determine the stress-separation relationship in the present study. Because the actual stress-separation relationship is not known a priori, possible stress-separation relationships were considered by varying the values of a^* and c^*, as shown in Figure 9. By choosing different values of a^* and c^*, the w_c value must be adjusted so that the fracture energy (or area under the curve) will remain the same. A bilinear relationship is used in the present study for simplicity; one can, of course, assume a more complex relationship for the stress-separation curve.

By trying different combinations of a^* and c^*, 25 bilinear σ-w curves with the same fracture energy (G_F) were generated. The values used in the 25 combinations were $a^* = 0.2$, 0.4, 0.6, 0.8, and 1.0 and $c^* = 0.1$, 0.3, 0.5, 0.7, and 0.9.

Figure 10 shows that the predicted load versus load-line deflection response is very sensitive to the shape of the stress-separation (σ-w) curve. It was found that the experimental result can be better reproduced using $a^* = 1.0$ and $c^* = 0.48$, as shown in Figure 8. There are no available data to assess the effects of asphalt grade, aggregate types and gradation, and different additives on the values for a^* and c^*.

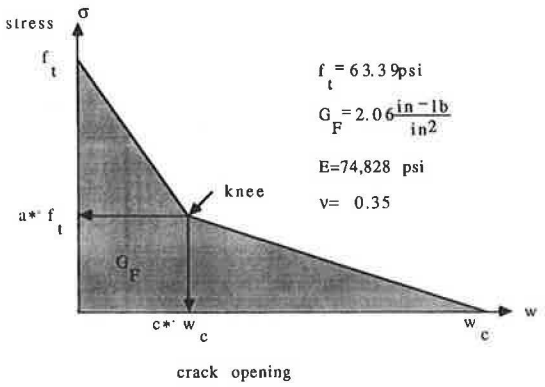

FIGURE 9 Bilinear stress-separation curve for numerical simulation.

TABLE 3 SUMMARIES OF MATERIAL PROPERTIES USED IN PRESENT STUDY

Temperatures (°F)	18	36	75	104	140
Tensile strength f_t (psi)	305.4	189.16	63.39	13.70	3.62
Fracture Energy G_F (lb/in)	4.726	4.413	2.06	0.364	0.065
Young's modulus E (Ksi)	483	268	75	29	9
Poisson's ratio	0.13	0.25	0.35	0.46	0.48
Characteristic length, L_{ch} (in)	24.45	33.03	38.36	56.22	44.31

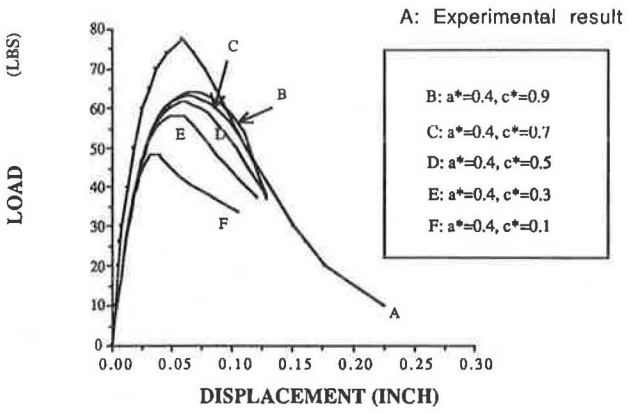

FIGURE 10 Numerical results of load-deflection curves using different stress-separation relationships.

An experimental program at Ohio State University is evaluating these effects.

Using the same stress-separation relationship, the load-deflection curves obtained for different notch-depth ratios (0.4 and 0.6) were found to be satisfactory. It can be concluded that the proposed stress-separation relationship is acceptable and that more experimental data, of course, are needed to obtain a more accurate relationship.

Development of the Process Zone

The stress distribution of the process zone at different loading stages is shown in Figure 11 for a notch-depth ratio of 0.2. The process zone starts to develop when the load is applied. It can be observed that at Stage 1, a small process zone has already developed. Note that no stress exceeds the maximum tensile strength (f_t) along the process zone. At the second stage, the cohesive crack propagates and the process zone is extended. When the peak load is reached (Stage 3), the stress distribution is quite different compared to the linear-elastic one. Nevertheless, the material along the process zone is still able to transfer stress even after the peak load is reached, and the traction free crack will not propagate until the fourth stage is reached.

Temperature Effects on *P*-δ and *P*-CMOD Curves

As shown in Figure 12, the behavior or asphalt concrete becomes more brittle when the temperature decreases; that is, the peak load is reached at a much smaller deformation at lower temperatures. This low-temperature–enhanced brittleness is mainly caused by the increase of Young's modulus and tensile strength values. Although the tensile strength, as well as the fracture energy, is higher at lower temperatures, for the same amount of thermal contractions and deformation (or displacement), asphalt concrete is more susceptible to thermal cracking during winter because of the brittleness enhanced by lower temperatures.

Temperature Effects on Fracture Parameters

By knowing the peak load value obtained from the proposed cohesive crack model, one can also calculate the critical stress intensity factor (K_{Ic}) at different temperatures.

The model prediction shown in Figure 13a indicates that the higher the temperature, the lower the critical stress intensity factor will be. This trend was also reported by Karakouzian (*14*) (see Figure 13b).

Among the various fracture parameters, the J-integral proposed by Rice in 1968 has been widely used (*15*). The J-integral is defined as a path-independent contour integral representing a nonlinear elastic energy release rate. By using the load versus load-line deflection curve obtained from the model, one can measure the area under the curve up to the peak load for different notch-depth ratios. Based on these measurements, U_T and thus J_{Ic} can be determined (*9*). Unlike the critical stress intensity factor, the critical J-integral was found to increase with temperature up to about 40°F and then decreases for much higher temperature (Figure 14a). A similar experimental observation was also reported by Dongre et al. (*16*), as shown in Figure 14b. It is, however, difficult to make conclusions for temperatures higher than 40°F because of the large dispersion observed in the experimental data. More experimental results are needed to verify the theoretical prediction at a higher temperature range.

With the proposed model and the aid of finite element analysis, one can also analyze the crack resistance of a pavement structure. For example, the effects of seasonal and daily thermal cycles, thermal gradients, thermal contraction of concrete slabs, and joint faulting on the performance of asphalt concrete overlay can be objectively analyzed, and the mechanisms that cause premature pavement failure can be better understood. Research results on these effects will be presented elsewhere.

CONCLUSIONS

1. By using the cohesive crack model, progressive crack development in asphalt concrete can be properly simulated. The effects of temperature on the crack resistance of asphalt concrete pavements can thus be objectively evaluated.
2. Based on the proposed model, the effect of temperature on the fracture toughness K_{Ic} can be correctly predicted. However, no definite conclusion can be made about the critical J-integral based on the theoretical predictions and the available experimental results.
3. In this study, the stress-separation (σ-w) relationships were determined using a back-calculation method and were assumed to be the same for various temperatures. To correctly evaluate the effect of temperature on the stress-separation curve, a direct uniaxial tensile test should be performed under different temperatures.
4. The proposed cohesive crack model is very promising in evaluating the temperature effect on the viscoelastic fracture response of asphalt concrete pavements.

ACKNOWLEDGMENTS

Partial support provided by the Ohio Department of Transportation and Illinois Tool Works, Inc., is gratefully appreciated.

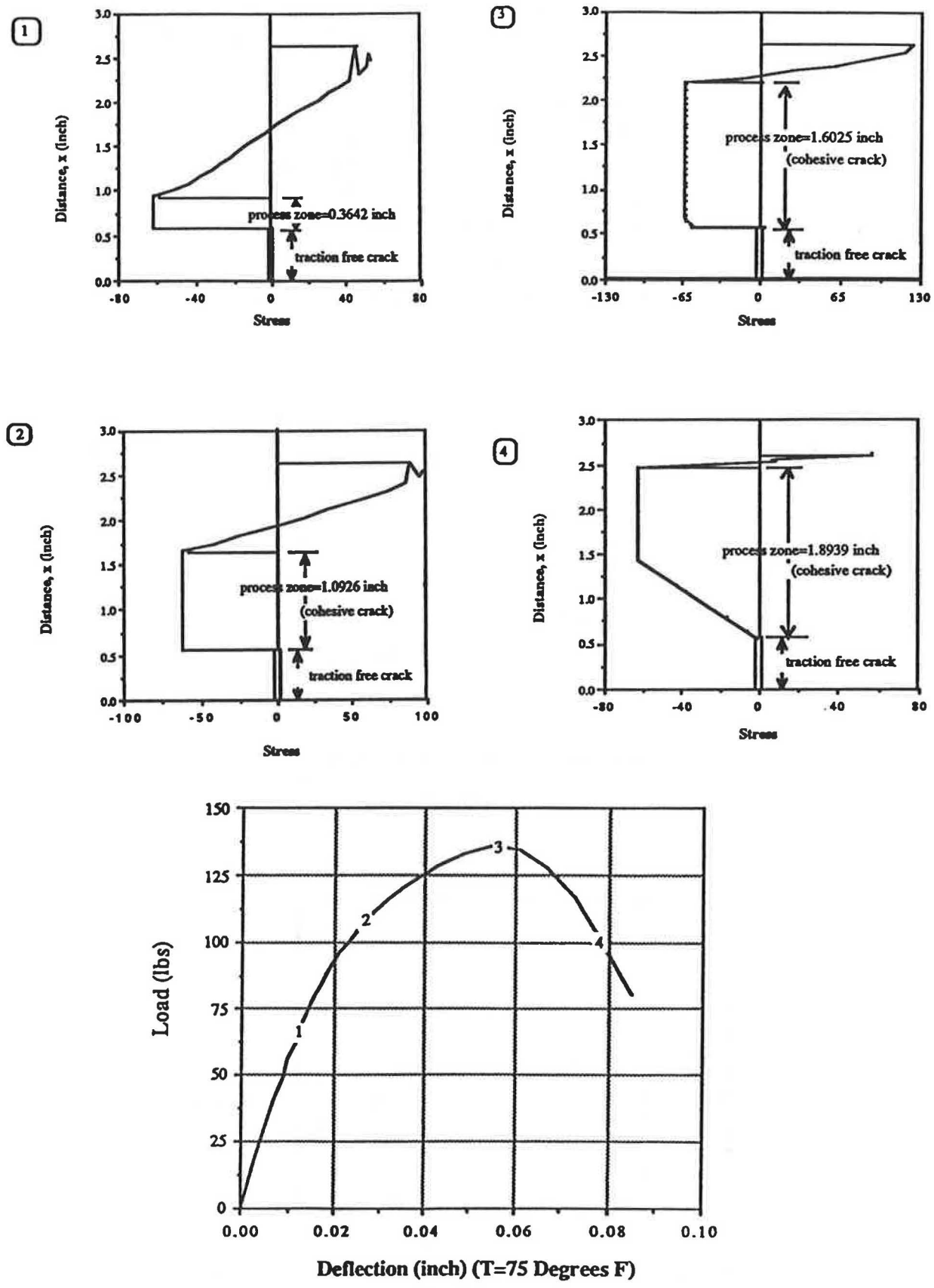

FIGURE 11 Development of process zone at different loading stages.

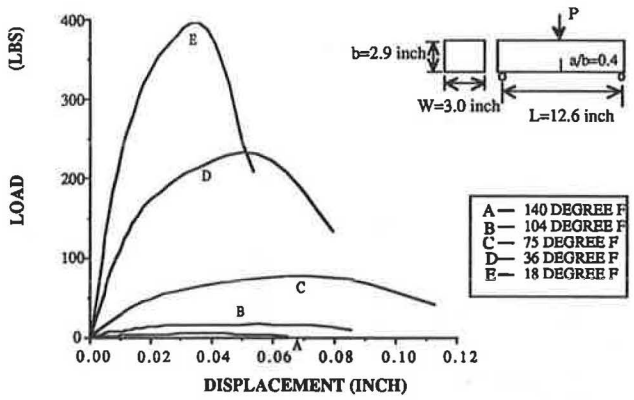

FIGURE 12 Effects of temperature on load-deflection curve ($a/b = 0.4$).

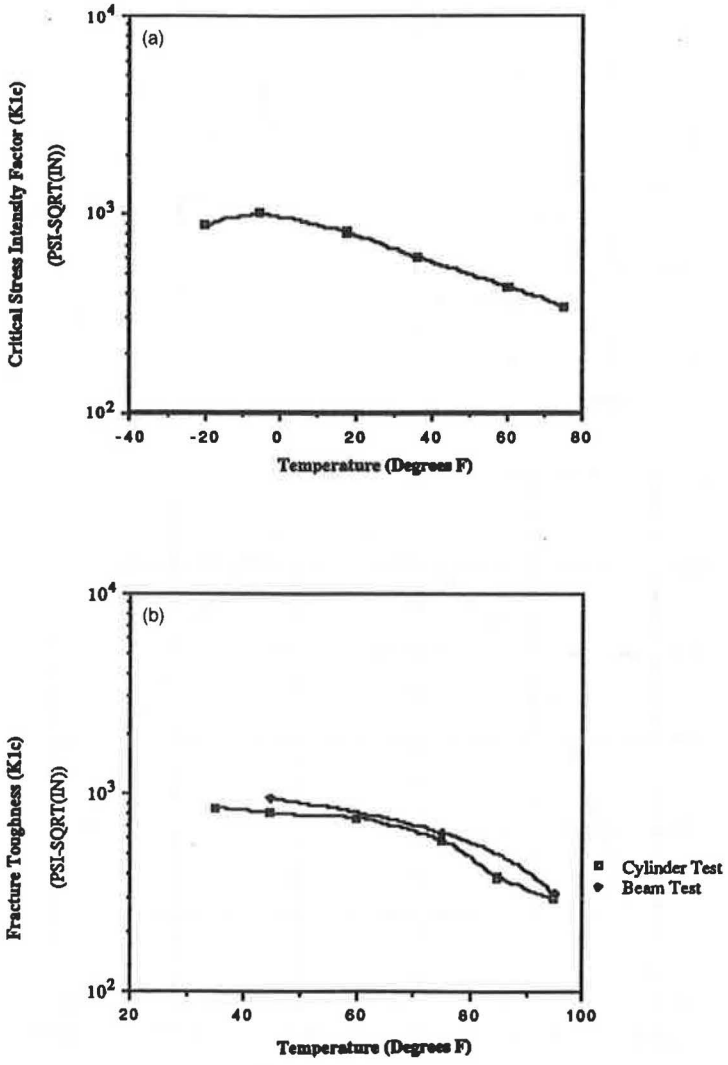

FIGURE 13 Effects of temperature on critical stress intensity factors (K_{Ic}). (a) Theoretical predictions (b) Experimental results

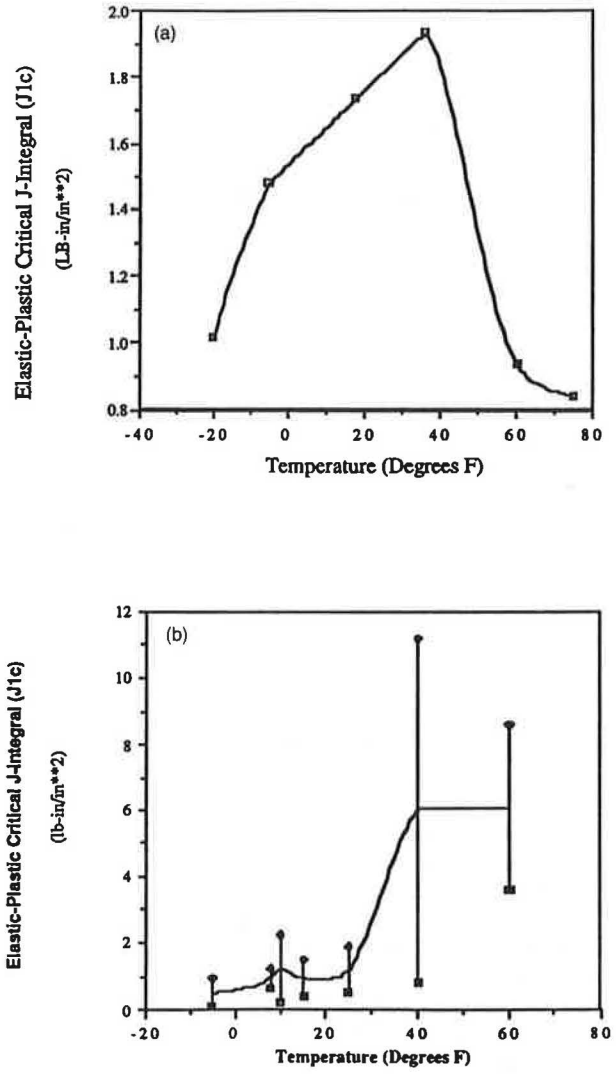

FIGURE 14 Effects of temperature on critical J-integral. (a) Theoretical predictions (b) Experimental results

REFERENCES

1. S. F. Brown. *Time-Dependent Behaviour of Bituminous Material.* Creep of Engineering Materials. Senior Lecture in Civil Engineering, University of Nottingham, England, 1978.
2. A. A. Griffith. Theory of Rupture. *Proc., 1st International Congress in Applied Mechanics*, 1924.
3. G. R. Irwin. Analysis of Stresses and Strains Near the End of a Crack Traversing a Plate. *Journal of Applied Mechanics*, Transaction ASME, Vol. 79, 1957, pp. 361–364.
4. E. Orowan. Energy Criterion of Fracture. *Welding Journal Research Supplement*, March 1955, pp. 157–160.
5. G. R. Irwin and J. A. Kies. Critical Energy Rate Analysis of Fracture Strength. *Welding Journal Research Supplement*, Vol. 33, 1954, pp. 193–198.
6. D. S. Dugdale. Yielding of Steel Sheets Containing Slits. *Journal of the Mechanics and Physics of Solids*, Vol. 8, 1960, pp. 100–108.
7. G. I. Barenblatt. The Mathematical Theory of Equilibrium of Crack in Brittle Fracture. *Advances in Applied Mechanics*, Vol. VII, 1962, pp. 55–129.
8. A. Hillerborg, M. Modeer, and P. E. Petersson. Analysis of Crack Formation and Crack Growth in Concrete by Means of Fracture Mechanics and Finite Elements. *Cement and Concrete Research*, Vol. 6, No. 6, Nov. 1976, pp. 773–782.
9. J. D. Perng. *Analysis of Crack Propagation in Asphalt Concrete Using a Cohesive Crack Model.* M.S. thesis. Department of Civil Engineering, Ohio State University, Columbus, 1989.
10. *Construction and Material Specification.* Department of Transportation, State of Ohio, Columbus, Jan. 1987.
11. *Mix Design Methods for Asphalt Concrete and Other Hot-Mix Types.* Manual Series No. 2, Asphalt Institute, May 1984.
12. J. W. Kennedy and W. R. Hudson. Application of the Indirect Tensile Test to Stabilized Materials. In *Highway Research Record 235*, HRB, National Research Council, Washington, D.C., 1968, pp. 36–48.
13. E. J. Yoder and M. W. Witczak. *Principles of Pavement Design.* John Wiley and Sons, Inc., New York, 1975.
14. M. Karakouzian. *A Simplified Method for Material Testing and Design of Pavement Systems.* Ph.D. dissertation. Ohio State University, Columbus, 1978.
15. J. R. Rice. A Path Independent Integral and the Approximate Analysis of Strain Concentration by Notches and Cracks. *Journal of Applied Mechanics*. Vol. 35, 1968, pp. 379–386.
16. R. Dongre, M. G. Sharma, and D. A. Anderson. Development of Fracture Criterion for Asphalt Mixes at Low Temperatures. In *Transportation Research Record 1228*, TRB, National Research Council, Washington, D.C., 1989, pp. 94–105.